A comparative study of Si-$BaSO_4$ and Si-$CaSO_4$ pyrotechnic time delay compositions

Shepherd M. Tichapondwa[1*], Walter W. Focke[1], John Gisby[2], Olinto Del Fabbro[1], Cheryl Kelly[3]

[1]Institute of Applied Materials, Department of Chemical Engineering, University of Pretoria, Lynnwood Road, Pretoria, South Africa

[2]National Physical Laboratory, Teddington, Middlesex, TW11 0LW, United Kingdom

[3]Research and Technology, AEL Mining Services, PO Modderfontein, 1645, South Africa

Abstract

Slow burning Si-$BaSO_4$ pyrotechnic delay compositions are employed commercially for intermediate to long time delays. However, there is very little information on this composition available in open literature. The reactivity of this composition was therefore characterized and compared to that of Si-$CaSO_4$. The Si-$BaSO_4$ composition supported combustion in the range of 20 to 60 wt.% Si in the bomb calorimeter. However, burning was only sustained between 20 and 40 wt.% Si in rigid aluminum tubes, with burning rates of between 8.4 and 16 mm s^{-1}. These values are comparable to those for the Si-$CaSO_4$ system (6.9 – 12.5 mm s^{-1}). However, the $CaSO_4$ based formulations tended to have higher energy output and produced more transient pressure compared to the barium sulfate compositions. Both formulations were insensitive to impact, friction and electrostatic discharge stimuli. The reaction products were a complex mixture that contained crystalline phases in addition to an amorphous phase. Although barium sulfate is insoluble in water and decidedly non-toxic, the reaction products produced by the Si-$BaSO_4$ compositions were found to release soluble barium ions when contacted with water. This ranged from 50 to 140 mg per gram of barium sulfate reacted.

* Corresponding author; e-mail: tichapondwa@gmail.com

Keywords silicon; barium sulfate; calcium sulfate; time delay; pyrotechnics

1. Introduction

Delay detonators are used extensively in mining, quarrying and other blasting operations in order to facilitate sequential initiation of the explosive charges in a pattern of boreholes [1]. The timing of the sequential initiation events are carefully chosen in order to control the fragmentation and throw of the rock being blasted. This approach also reduces ground vibration and air blast noise [1]. Both chemical and electronic time delay detonators are used to achieve the required time delays. The simplicity, ruggedness and low cost of pyrotechnic delays make them particularly attractive for high volume mining applications.

Pyrotechnic compositions consist of one or more oxidizer in combination with one or more fuel [2-4]. Some of the more common oxidizers used in pyrotechnic compositions include oxides and oxy salts of alkali, alkali earth or transition metals. The oxy salts are classified according to relevant anions, i.e. chlorates, perchlorates, nitrates, chromates and sulfates [2, 5]. These oxidizers may release oxygen to the reducing fuel via lattice destabilization, melting, sublimation and thermal decomposition [2, 6, 7]. The selection of an oxidizer for a given fuel is dependent on the desired energy output, reaction rate and the physical state of the reaction products [8]. Usually slow burning pyrotechnic reactions are obtained when the oxidizer releases oxygen at high temperatures and undergoes endothermic decomposition [2, 8]. This is exemplified by barium sulfate as oxidizer in slow burning silicon based pyrotechnic delay compositions [1, 9].

The Si-$BaSO_4$ composition was patented by Beck and Flanagan [1]. It is commercially used in intermediate to slow delay time delay applications. Replacement of the barium sulfate by calcium sulfate was recently reported [10]. McLain [2] states that the crystal form and crystal defects present in pyrotechnic reagents influence the reactivity of

pyrotechnic compositions. Barium sulfate and calcium sulfate both have orthorhombic crystal structures [11]. The reactivity of pyrotechnic compositions utilizing an oxy salt oxidizer depends primarily on the nature of the anion [6]. However, the cation potentially also plays a role [12, 13] as this study showed by characterizing the Si-$BaSO_4$ composition and comparing its performance to that of Si-$CaSO_4$.

2. Experimental

Materials

The properties of the materials used to prepare the different compositions are shown in Table 1. X-ray diffraction (XRD) analysis confirmed that all the raw materials were of high purity. Surface area was measured with a Micrometrics Tristar II BET. Laser diffraction particle sizing was performed with a Mastersizer Hydrosizer 2000 instrument using water as the dispersion medium. Figure 1 shows scanning electron microscopy (SEM) pictures of the barium sulfate and silicon. The samples were first coated with gold and then imaged using a JEOL JSM 5800 SEM.

Table 1. Standard enthalpy of formation (ΔH_f°), volume-based median particle size (D_{50}) and BET surface areas of the raw materials used

	Supplier (Grade)	ΔH_f° (kJ mol^{-1})	D_{50} (μm)	BET (m^2 g^{-1})
Barium sulfate	Sachtleben (Blank Fixe N)	- 1465	4.31	0.82
Calcium sulfate	Alfa Aesar	- 1433	4.05	3.78
Silicon	Millrox (Type 4)	-	1.85	11.03

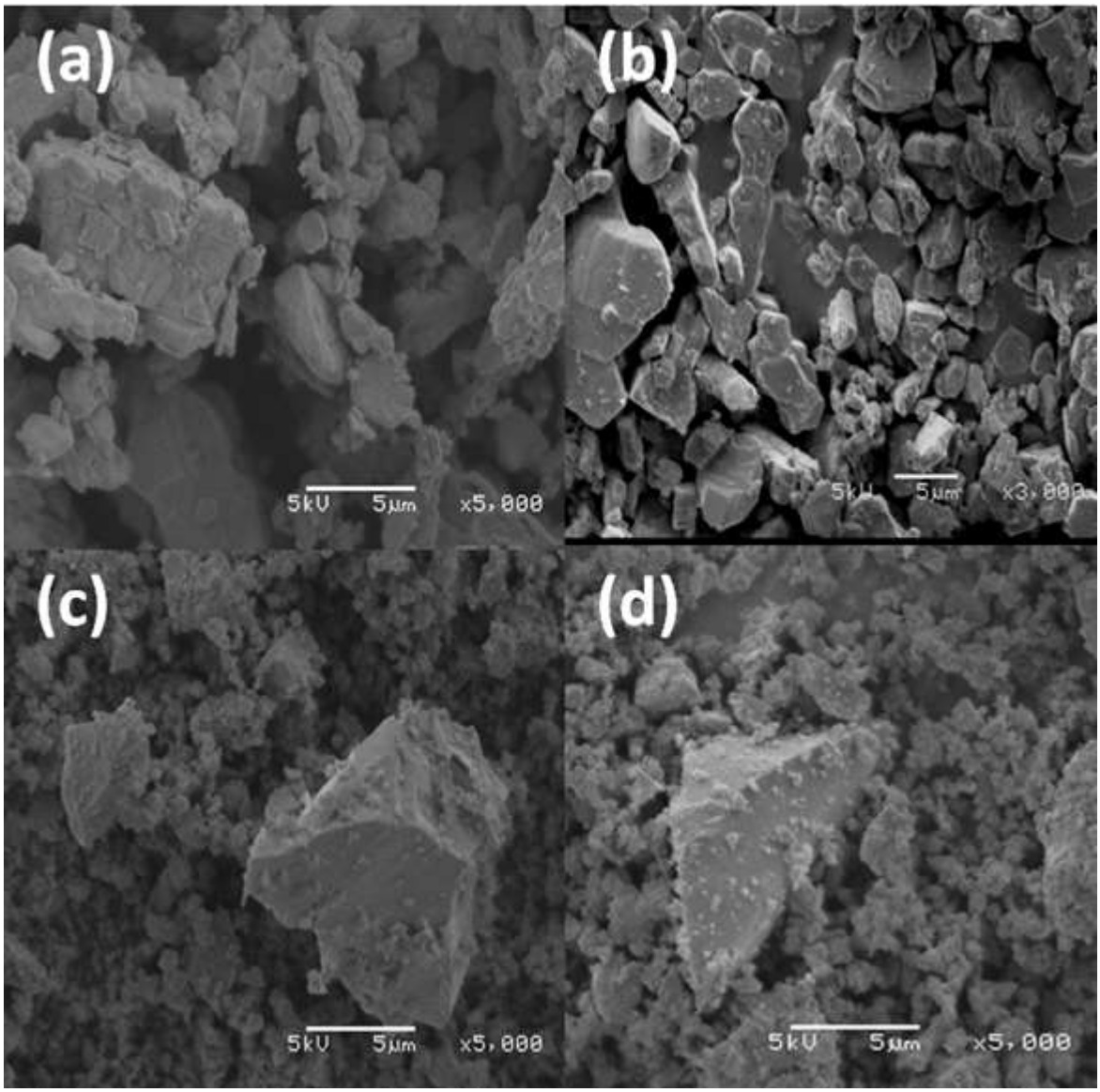

Figure 1. SEM pictures of the raw materials used in the experiments. Barium sulfate (a) and (b); silicon (c) and (d).

Characterization

Thermogravimetric analysis (TGA) was performed on a Mettler Toledo A851 TGA/SDTA using the dynamic method. About 15 mg of powder sample was placed in an open 70 µL alumina pan. Temperature was scanned from 25 to 1300 °C at a rate of 10 °C min^{-1} with nitrogen flowing at a rate of 50 mL min^{-1}. Three runs were carried out for each sample.

Enthalpy measurements were carried out using a Parr 6200 calorimeter utilizing a 1104B 240 mL high strength bomb. Tap compacted test compositions (2 g) were initiated

using 0.2 g of a proprietary starter. The latter was ignited with an electrically heated 30 gauge nichrome wire. The tests were carried out in a 3.0 MPa helium atmosphere. The variation of pressure with time was followed using a National Instruments piezoelectric transducer. A Parr Dynamic Pressure Recording System was used for data collection. The recording frequency was 5 kHz and 30000 data points were captured per test. Each composition was tested at least three times. The starter composition (0.2 g) was tested on its own. The pressure rise was too low to be measurable in the bomb calorimeter. The energy output was 1.5 MJ kg^{-1} and the reported experimental values were corrected for this.

X-ray diffraction (XRD) analyses were performed on a BRUKER D8 ADVANCE diffractometer with 2.2 kW CuKα radiation (λ=1.54060 nm) fitted with a LynxEye detector with a 3.7º active area. Samples were scanned in reflection mode in the angular range 2° to 70° 2θ at a rate of 0.01° s^{-1}. The generator settings were 40 kV and 40 mA. Data processing and analysis were carried out using the BRUKER DIFFRACPlus - EVA evaluation program. Quantitative XRD analyses were performed according to the Rietveld method using DIFFRACPlus TOPAS software. The powdered residues were spiked with known proportions of corundum to facilitate determination of the amorphous content using procedure described by Ward and French [14].

Single point sulfur analyses were performed on an Eltra CS 800 double dual range carbon-sulfur analyzer. Samples of the reaction products weighing ca. 0.2 g were milled and sieved to <75 µm. The samples were homogenized by slow rotation in a ceramic crucible with iron and tungsten chips. The instrument was calibrated using the Euronorm-CRM 484-1 Whiteheart malleable iron, Euronorm-CRM 058-2 sulfur steel and Euronorm-CRM 086-1 carbon steel standards. The instrument stability was monitored using the Council for Geoscience laboratory in-house soil reference standards. The sulfur detection limit was 0.009 wt.%.

Sensitivity testing was performed on 30 wt.% silicon compositions using the standard procedures described in MIL-STD-1751A [15]. The impact and friction sensitivities were determined with an OZM Research BFH-10 BAM fall hammer impact sensitivity tester and an OZM Research FSKM 50-20K BAM friction tester, respectively. An OZM Research ESD 2008A small-scale electrostatic spark sensitivity tester was used for electrostatic discharge (ESD) sensitivity. The nominal ignition thresholds were determined using the Bruceton 50% method as described in MIL-STD-1751A.

A SPECTRO ARCOS inductively coupled plasma optical emission spectrometer (ICP-OES) was used to establish the amount of dissolved barium after the solid residue obtained from the combustion of Si-$BaSO_4$ compositions was contacted with water. Calibration with a barium standard (ICP grade) was carried out before running the leached samples. Each sample was measured three times and the average ICP value was recorded.

Composition and delay element preparation

The silicon fuel and $BaSO_4$ or $CaSO_4$ oxidants powders were mixed by brushing them several times through a 75 μm sieve. The compositions were pressed into 25 mm long aluminum tubes with an internal diameter of 3.6 mm and a wall thickness of 1.45 mm. The filling process started with two increments of a proprietary starter composition pressed with a 100 kg load. This was followed by repeated steps of adding two increments of the delay composition and pressing it with the same load until the tube was filled. The densities achieved were 57±3 % of the theoretical maximum density (TMD).

Burning rate measurements

The burning rates were determined using commercial detonator assemblies. These comprised an initiating shock tube coupled to a rigid aluminum time delay element contained in an

aluminum shell. This outer shell contained increments of lead azide primary explosive and pentaerythritol tetranitrate (PETN) as the secondary explosive. The actual delay time was determined using the method previously described [10, 16]. In this method the shock tube is ignited using a firing device and the resultant flash is recorded with a photoelectric cell. This signal is sent to a timer as the initiating signal. After detonation, a pressure transducer sends another signal to the timer and marks the end point of the timing sequence.

Determination of the amount of dissolved barium

Approximately 2 g of either the solid reaction products obtained after combusting various Si-$BaSO_4$ compositions in inert helium atmosphere in the bomb calorimeter, or pure barium sulphate, was contacted with 10 mL of de-ionized water. The mixture was agitated using an orbital shaker for 1 month and then filtered. The resultant solution was analysed for the barium using inductively coupled plasma optical emission spectroscopy (ICP-OES).

3. Results

Thermal behavior of reactants in nitrogen

Figure 2 shows the thermal behavior of silicon, barium sulfate and calcium sulfate in a nitrogen atmosphere. The silicon showed no significant change in mass below 600 °C. However, a mass increase associated with the formation silicon nitride was noted above 600 °C. Barium sulfate was stable in the temperature range tested with only a slight mass decrease observed above 1200 °C. The thermal decomposition of $BaSO_4$ occurs in the temperature range 1125 to 1400 °C and takes place according to Scheme I [9, 17, 18]. The ultimate theoretical mass loss is ca. 34.4%. The decomposition of anhydrous $CaSO_4$ proceeds in a similar manner in the range 1080 to 1300 °C [9, 10, 19].

$BaSO_4$ (s) → BaO (s) + SO_3 (g) (1)

$BaSO_4$ (s) → BaO (s) + SO_2 (g) + ½ O_2 (g) (2)

Scheme I. Barium sulfate thermal decomposition pathways

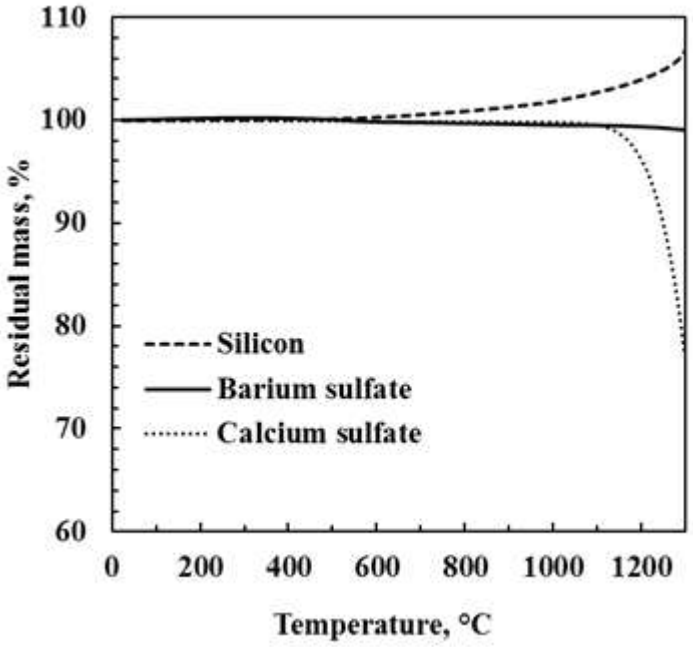

Figure 2. TGA results for silicon, barium sulfate and calcium sulfate recorded in nitrogen atmosphere.

Barium sulfate and calcium sulfate release the same molar amount of oxygen. However, barium sulfate is more thermally stable and thus releases it at a higher temperature.

Experimental and Theoretical Energy output measurements

Figure 3 compares the effect of fuel content on the energy output of the Si-$BaSO_4$ and Si-$CaSO_4$ formulations in a helium atmosphere. Whereas calcium sulfate supports combustion in the range of 30-70 wt.% silicon, barium sulfate only burns in the 20 to 60 wt.% silicon range. The energy outputs for both formulations decreased approximately linearly with increase in Si content. Compared to calcium sulfate, barium sulfate-based compositions had lower

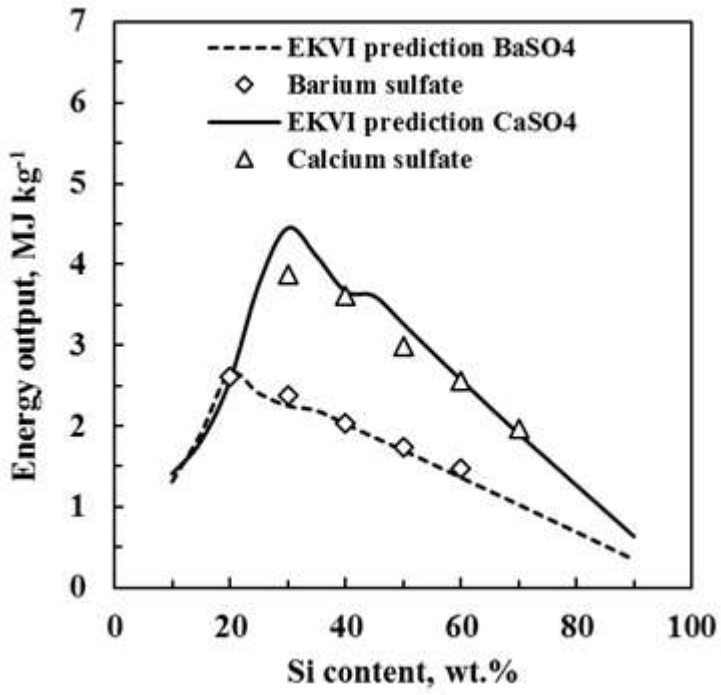

Figure 3. Comparison of energy outputs obtained from the bomb calorimeter measurements for the Si-$CaSO_4$ and Si-$BaSO_4$ systems and EKVI simulations in helium atmosphere.

energy outputs (1.42 – 2.63 MJ kg^{-1}). The highest energy outputs were observed at 20 wt.% Si and 30 wt.% Si for the Si-$BaSO_4$ and Si-$CaSO_4$ respectively. These compositions correspond to the ideal stoichiometry for both formulations and are similar to previously reported trends [3]. Calculated exothermicity values from the EKVI program for both the Si-$BaSO_4$ and Si-$CaSO_4$ systems were in reasonable agreement with the measured heats of reaction recorded using the bomb calorimeter. The maximum deviation from the predicted value was 7% for the S-$BaSO_4$ system and 15% for the Si-$CaSO_4$ combination. This suggests that the metal-oxidant reactions proceeded via the thermodynamically favored pathways. Figure 4 compares the predicted adiabatic reaction temperatures of the two systems. The Si-$BaSO_4$ compositions generated lower theoretical adiabatic temperatures compared to Si-$CaSO_4$. The highest temperatures were recorded at the stoichiometric composition for both formulations.

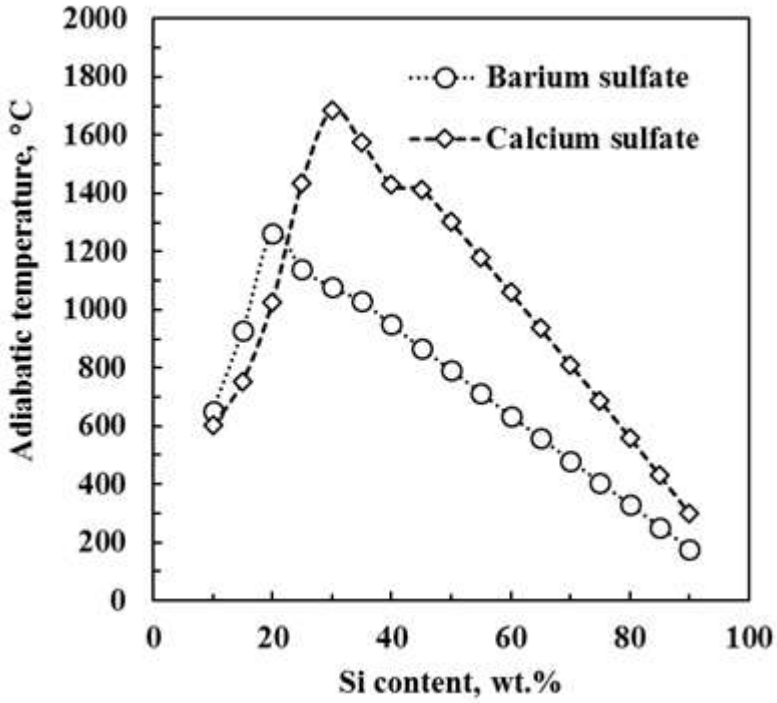

Figure 4. Comparison of the predicted adiabatic combustion temperature at different stoichiometries for both Si-$CaSO_4$ and Si-$BaSO_4$ systems using EKVI software.

Pressure – time analysis

Figure 5 and Table 2 report the pressure-time data obtained with bomb calorimetry. The indicated pressure readings are relative to the initial 3.0 MPa helium pressure. Above 30 wt.% silicon the rate of pressure rise, and the maximum peak pressure, decreased with increasing silicon content in accordance with the energy output trend. Based on the pressure-time parameters listed in Table 2, it can be concluded that Si-$CaSO_4$ is more reactive than corresponding Si-$BaSO_4$ formulations.

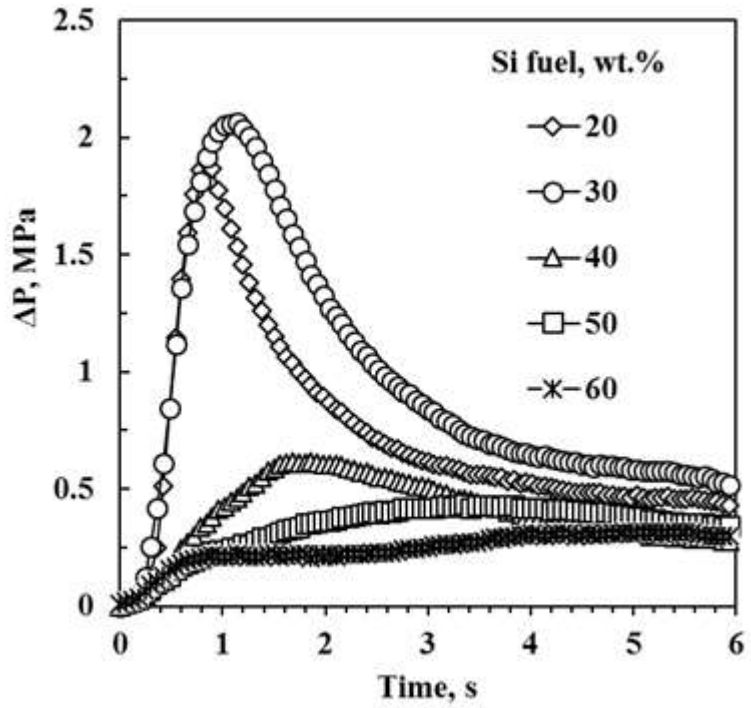

Figure 5. Pressure increase with time for different Si-$BaSO_4$ compositions during the bomb calorimetry experiments in a helium atmosphere.

Table 2. Summary of the parameters extracted from pressure-time profiles of Si-$CaSO_4$ and Si-$BaSO_4$ compositions with varying silicon fuel content

	Barium sulfate			**Calcium sulfate**		
Si content (wt.%)	P_{max} (MPa)	t_{max} (s)	dP/dt_{max} (MPa s^{-1})	P_{max} (MPa)	t_{max} (s)	dP/dt_{max} (MPa s^{-1})
20	1.89	0.84	5.43	-	-	-
30	2.07	1.14	4.44	2.06	1.14	4.45
40	0.61	1.68	0.75	1.76	1.20	3.08
50	0.434	3.36	0.39	1.41	1.26	1.82
60	0.32	5.04	0.44	0.65	1.92	0.60
70	-	-	-	0.49	2.04	0.40

Burning Rates

The effect of stoichiometry on the burning rate for both the Si-$BaSO_4$ and Si-$CaSO_4$ systems is shown in Figure 6. Although combustion of the Si-$BaSO_4$ system was sustained in the range of 20-60 wt.% Si in the inert atmosphere inside the bomb calorimeter, burning was

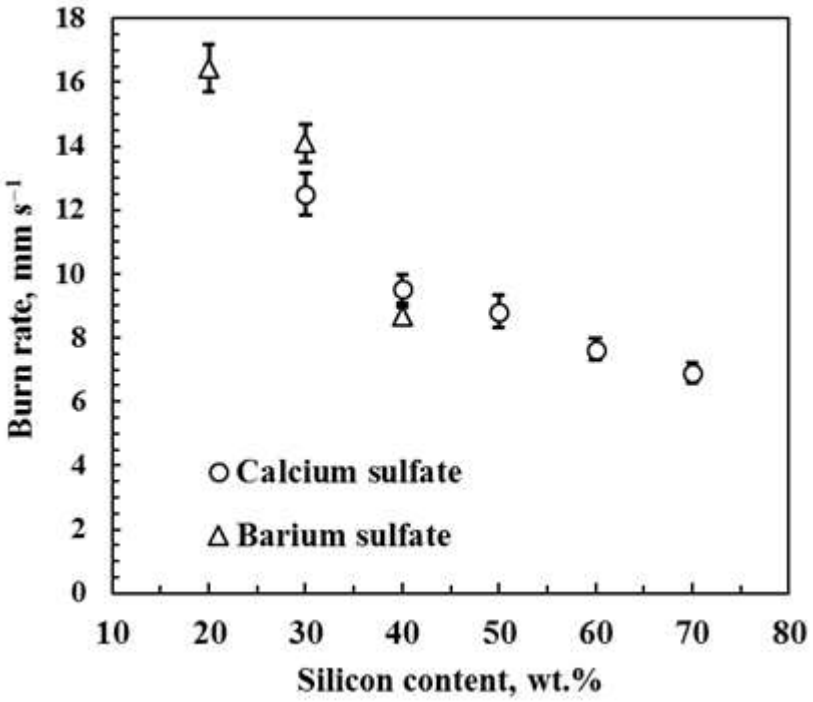

Figure 6. Effect of fuel content on the burning rate of Si-$BaSO_4$ and Si-$CaSO_4$ compositions.

only sustained in the range of 20 to 40 wt.% Si in the rigid aluminum tubes. This is attributed to higher heat losses experienced by compositions burning inside the tubes owing to more intimate contact with the conductive metal surface and a greater surface to volume ratio. In order to reduce such heat losses, Beck and Flanagan [1] tested compositions compacted into thin-walled (1 mm) rectangular stainless steel channels with larger internal dimensions (6 mm × 10 mm). In this scenario compositions containing as much as 55 wt.% Si propagated. Calcium sulfate based compositions had a wider burning range (30-70 wt.% Si). The burning rate decreased with increase in silicon content for both systems. The composition containing 20 wt.% Si-$BaSO_4$ composition burned fastest (16.0 mm s^{-1}) whilst the 40 wt.% Si was the

slowest with a burn rate of 8.4 mm s^{-1}. These values are similar to those reported for the Si-$CaSO_4$ compositions (6.9 – 12.5 mm s^{-1}) [10]. It should be noted that the burning rates recorded for the Si-$BaSO_4$ composition in these tests were higher than literature values (4-9 mm s^{-1}) [1, 20]. Likely causes for the discrepancy include differences in material of construction [21] and in the properties of the reagent materials, e.g. particle size, surface area, material history, purity and contaminants present [22].

XRD analysis of reaction products

Quantitative X-ray diffraction (XRD) analysis performed on the reaction products of the Si-$BaSO_4$ collected from the bomb calorimeter are reported in Table 3. The XRD diffractograms revealed a significant amount of an amorphous phase with quartz (SiO_2) and unreacted silicon as the only crystalline products. The presence of trace amounts of bismuth metal and bismuthinite (Bi_2S_3) are attributed to the proprietary bismuth oxide-based starter that was used for ignition. Similar observations were made for the Si-$CaSO_4$ compositions. No barium sulfate was detected regardless of the initial composition. This was expected as the compositions were fuel rich and the reaction temperatures exceeded the decomposition temperature of barium sulfate.

Sulfur analyses of the solid reaction residues (Table 3) allowed determination of the sulfur content of the amorphous phase. Between 50 and 70 % of the initial sulfur was retained in the amorphous phase depending on the initial stoichiometry. If it is assumed that no impurities were present in the reactants and that SO_2 was the only gas formed, sulfur mass balances enable estimation of the amount of gas produced by the reaction (Table 3). Depending on the stoichiometry, the gas evolved at standard temperature and pressure, ranged between 17.8 and 31.6 $cm^3\ g^{-1}$. The corresponding SO_2 estimates for $CaSO_4$ compositions ranged from 29.2 to 67.5 $cm^3\ g^{-1}$ [10]. Thus both compositions released more

than 10 cm^3 g^{-1} gas, the value regarded as an upper limit for classification as a gasless composition [23].

Table 3. Quantitative analysis of the reaction products identified from the Si–$BaSO_4$ pyrotechnic composition using XRD as well as an analysis of the total sulfur content in the solid products

Phase	**Formula**	**20**	**30**	**40**	**50**	**60**
Silicon	Si	4.9	13.9	26.1	36.4	45.7
Quartz	SiO_2	8.0	7.1	11.9	11.4	5.4
Bismuth	Bi	2.1	1.9	2.7	2.7	1.7
Bismuthinite	Bi_2S_3	2.9	2.6	2.1	1.9	1.1
Amorphous		82.0	74.6	57.3	47.8	46.1
Sulfur analysis	wt.%	8.6	5.6	6.2	3.5	3.1
Gas evolved	cm^3 g^{-1} (STP)	20.1	31.6	16.6	25.3	17.8

Simulated reaction products

Table 4 presents equilibrium product spectra predicted by EKVI simulations of the Si-$BaSO_4$ system. The reaction in all compositions was essentially gasless. The exception is the 10 wt.% silicon composition where S_2 gas is predicted and unreacted solid $BaSO_4$ was expected. For compositions above 10 Si wt.% the solid phases predicted were SiO_2, BaS, $BaSiO_3$, SiS and unreacted silicon. Interestingly, SiS is formed and no BaS is found in the products of the 30 wt.% composition. Further analysis suggests that the formation of SiS is favored when the reaction products end up in a molten state. Below its melting temperature, approximately

1090 °C, SiS is not formed. The products predicted by EKVI are in accord with the experimental observations if the BaS, $BaSiO_3$ and SiS form the detected amorphous phase.

Table 4. Product spectrum and adiabatic temperature (T_{ad}) predicted with the EKVI thermodynamics code for the Si-$BaSO_4$ system

	10	**20**	**30**	**40**	**50**	**60**	**70**	**80**	**90**
S_2 (g)	5.3	-	-	-	-	-	-	-	-
$BaSiO_3$ (s)	52.3	11.4	64.0	-	-	-	-	-	-
SiO_2 (s)	7.2	36.6	9.0	30.9	25.7	20.6	15.4	10.3	5.2
SiS (s)	-	2.7	18.0	-	-	-	-	-	-
BaS (s)	-	49.3	-	43.5	36.3	29.0	21.8	14.5	7.3
Si (s)	-	-	8.9	25.6	38.0	50.4	62.8	75.2	87.6
$BaSO_4$ (s)	35.2	-	-	-	-	-	-	-	-
T_{ad} (°C)	654	1262	1078	949	793	635	482	329	178

Owing to the limited data for barium silicate phases available in the EKVI software, simulations of the Si-$BaSO_4$ reaction were also carried out using MTDATA software. Table 5 shows predicted adiabatic reaction temperatures and product spectra. The barium silicate phases predicted were $Ba_2Si_3O_8$ and $BaSi_2O_5$ rather than the $BiSiO_3$ phase predicted by EKVI. All the other product compositions were similar to those predicted by EKVI with the exception of SiS which was not present. A comparison of the adiabatic reaction temperatures determined by the two software programs shows that they were nearly identical.

Table 5. Product spectrum and adiabatic temperature (T_{ad}) predicted with MTDATA software for the Si-$BaSO_4$ system

	10	**20**	**30**	**40**	**50**	**60**	**70**	**80**	**90**
$Ba_2Si_3O_8$ (s)	62.7	-	-	-	-	-	-	-	-
$BaSi_2O_5$ (s)	-	14.6	3.5	0.1	-	-	-	-	-
SiO_2 (s)	-	34.5	34.3	30.8	25.7	20.6	15.4	10.3	5.1
BaS (s)	0.5	50.9	49.0	43.5	36.3	29.0	21.8	14.5	7.3
Si (s)	-	-	13.1	25.6	38.0	50.4	62.8	75.2	87.6
$BaSO_4$ (s)	36.5	-	-	-	-	-	-	-	-
T_{ad} (°C)	631	1214	1097	949	793	635	482	329	177

Sensitivity Testing

Knowledge of the sensitivity to impact, friction and ESD stimuli are important when processing, handling and transporting the compositions. These were evaluated for the two 30 wt.% silicon compositions. No ignition was observed at the highest settings available for both the impact and friction tester (98 J for impact and 360 N for friction). Therefore, both compositions were classified as insensitive to impact and friction stimuli in accordance to the UN recommendations on the transportation of dangerous goods [24]. The calcium sulfate composition was more sensitive to electrostatic discharge (ESD) (118±46 mJ) compared to barium sulfate (145±26 mJ). Both formulations were classified as insensitive to ESD given that the approximate maximum ESD energy developed by the average person at 200 pF and 25 kV is in the order of 60 mJ [25]. It should be noted that humans are capable of acting as conduits passing higher ESD energy from other objects.

4. Discussion

Silicon dioxide and unreacted silicon were the only crystalline phases detected in the predominantly amorphous solid residue left by the Si-$BaSO_4$ reaction. Beck [20] previously reported that the residue is X-ray amorphous. Previous studies have established that the barium silicate system, xBaO-(100 - x)SiO_2, has a glass forming region around x = 25-40 [26, 27]. In this study the composition of the amorphous phase was assessed based on TG and XRD results, sulfur analysis data, EKVI and MTDATA simulations as well as a previously reported reaction mechanism [10]. It is postulated that the amorphous phase is a composite mixture of any of the following phases: $BaSiO_3$, $Ba_2Si_3O_8$, $BaSi_2O_5$, BaS, SiO_2 and $BaSO_4$. The SiS predicted by EKVI was not considered as a component in the amorphous phase since the analyzed residual material would have cooled to room temperature and the SiS should have transformed to a more stable form. The unreacted silicon was also not considered as part of the amorphous phase as the crystalline amounts quantified by XRD were almost identical to those predicted by the software packages. Barium sulfide accounted for most of the sulfur, with the balance present in the form of with unreacted amorphous $BaSO_4$ [28]. It should be noted that the barium silicate compounds are essentially combinations of SiO_2 and BaO units; this is a well-known system that has been extensively studied [26, 27, 29-31]. The combination of these two compounds in various mole ratios generates seven possible solid phases, i.e. Ba_3SiO_5, Ba_2SiO_4, $BaSiO_3$, $Ba_2Si_3O_8$, $Ba_5Si_8O_{21}$, $Ba_3Si_5O_{13}$ and $BaSi_2O_5$ (Figure 7) [31].

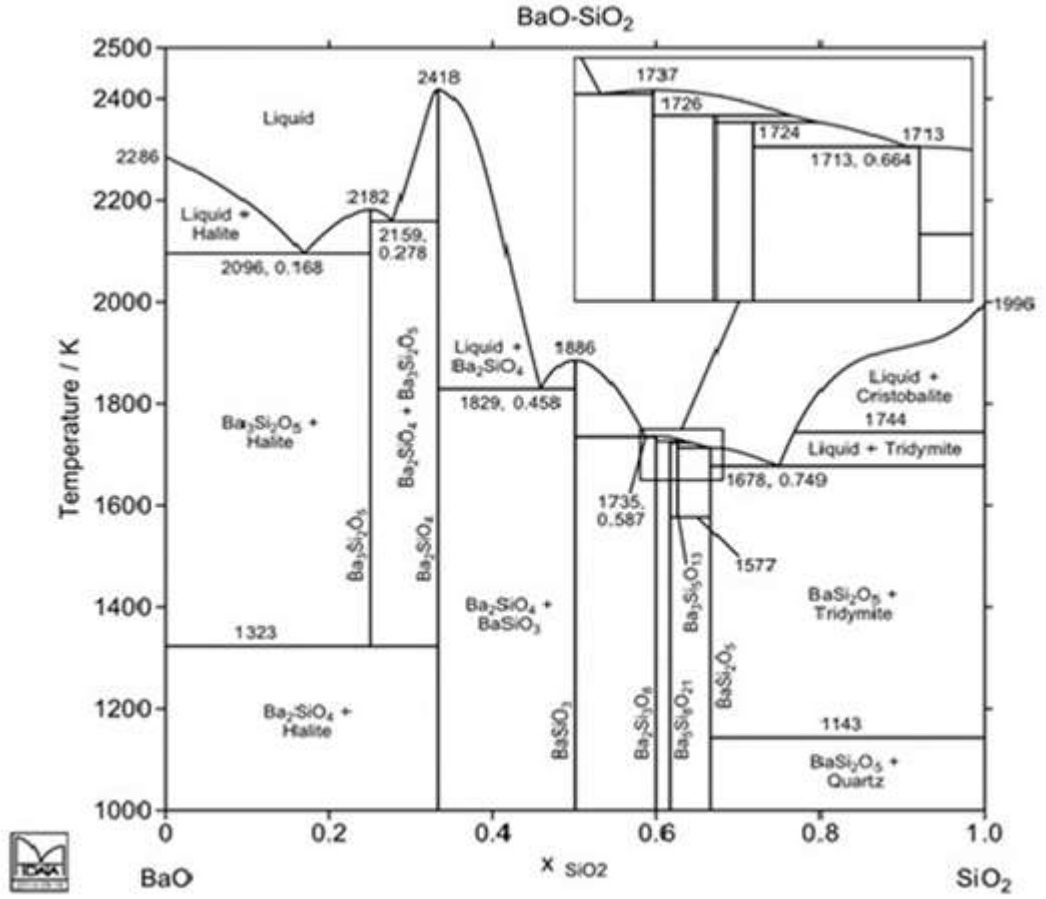

Figure 7. Phase diagram for the system BaO-SiO_2 produced using the MTDATA software.

Although barium sulfate is insoluble in water, its reaction with silicon has the potential of producing soluble reaction products. The barium containing reaction products predicted by EKVI and MTDATA simulations are to a certain degree soluble in water. Barium sulfide has a solubility of ca. 9 g per 100 mL of water at 20 °C. Whilst, barium silicates are not all stable in the presence of water and over time barium may leach. They undergo hydration reactions hydrate and may partially decompose to form free $Ba(OH)_2$ [32]. The latter is soluble and toxic. The solid residue obtained after burning the various compositions was contacted with water. All the residues produced a distinct "rotten egg" smell which confirmed the presence of sulfide compounds as these are known to release H_2S due to hydrolysis in water. Analysis

of the resulting leachate using ICP-OES showed dissolved barium in the range of 50 to 140 mg per gram of barium sulfate reacted for the different compositions. Pure barium sulfate was also contacted with water and virtually no barium was detected in the resultant solution. This confirmed that the barium detected was due to products formed. The degree of barium dissolution was generally low, this was thought to result from the barium sulfide being trapped within the glassy amorphous silicate phase. Although the amount of dissolved barium was relatively low, it should be noted that the maximum contaminant level (MCL) of barium in drinking water is 2 mg L^{-1} [33]. Acute exposure at levels above this can potentially cause gastrointestinal disturbances and muscular weakness. Long-term exposure results in hypokalemia, which can result in ventricular tachycardia, hypertension and/or hypotension, muscle weakness, and paralysis [34].

Conclusions

The Si-$BaSO_4$ composition was characterized and compared to that of silicon and calcium sulfate. Barium sulfate has a higher thermal degradation temperature than calcium sulfate. In both systems the energy output, the pressure generated, the amount of gas generated and the burning rate decreased with increasing silicon content. Except for the burning rates, these performance indices were lower with barium sulfate as the oxidant. The reaction residues for the $BaSO_4$ compositions were essentially XRD-amorphous but minor amounts of crystalline SiO_2 and unreacted Si were detected. EKVI and MTDATA thermodynamic simulations for the Si-$BaSO_4$ system provided insight into the possible composition of the amorphous phase. The solid reaction products formed by the Si-$BaSO_4$ compositions released soluble barium ions when contacted with water. Both systems were relatively insensitive to impact, friction and electrostatic discharge stimuli at a silicon content of 30 wt.%.

Acknowledgements

This work is based on the research supported in part by AEL Mining Service and by the National Research Foundation of South Africa (Grant 83874). The opinions, findings and conclusions or recommendations expressed in this publication are those of the authors, and neither AEL Mining Services nor the NRF accept any liability whatsoever in this regard.

References

[1] Beck M.W. and J. Flanagan. 1992. Delay composition and device. U.S. Patents #5147476.

[2] Mclain JH. Pyrotechnics from the Viewpoint of Solid State Chemistry. Philadelphia: The Franklin Institute Press; 1980.

[3] Berger B. 2005 Parameters Influencing the Pyrotechnic Reaction. *Propellants, Explosives, Pyrotechnics*. 30:27-35.

[4] Danali SM, Palaiah RS, Raha KC. 2010 Developments in Pyrotechnics. *Defence Science Journal*. 60:152-8.

[5] Steinhauser G, Klapötke TM. 2008 "Green" Pyrotechnics: A Chemists' Challenge. *Angewandte Chemie - International Edition*. 47:3330-47.

[6] Conkling J.A. 1985. Chemistry of Pyrotechnics, Basic Principles and Theory. New York. Marcel Dekker, Inc.

[7] Laye PG, Charsley EL. 1987 Thermal Analysis of Pyrotechnics. *Thermochimica Acta*. 120:325-49.

[8] Conkling J.A. 2001. Pyrotechnics. Kirk-Othmer Encyclopedia of Chemical Technology. New Jersey. John Wiley and Sons Inc.

[9] Stern K and E Weise. 1966. High temperature properties and decomposition of inorganic salts. Part 1. Sulfates. Defense Technical Information Center Document.

[10] Tichapondwa SM, Focke WW, Del Fabbro O, Kelly C. 2014 Calcium Sulfate as a Possible Oxidant in “Green” Silicon-based Pyrotechnic Time Delay Compositions. *Propellants, Explosives, Pyrotechnics*. n/a-n/a.

[11] Caspari W. 1936 Calcium sulphate hemihydrate and the anhydrites. I. Crystallography. Proceedings of the Royal Society of London Series A, *Mathematical and Physical Sciences*. 155:41-8.

[12] Spice J and L.Staveley. 1949. The propagation of exothermic reactions in solid systems, part II. Heats of reaction and rates of burning. *Journal of the Society of Chemical Industry*.68:348-55.

[13] Rugunanan R.A. 1992. Intersolid pyrotechnic reactions of silicon. *PhD Thesis*, Rhodes University.

[14] Ward CR, French D. 2006 Determination of glass content and estimation of glass composition in fly ash using quantitative X-ray diffractometry. *Fuel*.85:2268-77.

[15] Defense UDo. MIL-STD-1751A. US Department of Defense Test Method Standard, Safety and Performance Tests for the Qualification of Explosives (High Explosives, Propellants, and Pyrotechnics). 2001.

[16] Ilunga K, del Fabbro O, Yapi L, Focke WW. 2011 The effect of Si-Bi_2O_3 on the ignition of the Al-CuO thermite. *Powder Technology*. 205:97-102.

[17] Holt BD, Engelkemeir AG. 1970 Thermal decomposition of barium sulfate to sulfur dioxide for mass spectrometric analysis. *Analytical Chemistry*. 42:1451-3.

[18] Mohazzabi P, Searcy AW. 1976 Kinetics and thermodynamics of decomposition of barium sulphate. *Journal of the Chemical Society, Faraday Transactions 1: Physical Chemistry in Condensed Phases*. 72:290-5.

[19] Newman ES. 1941 Behavior of calcium sulfate at high temperatures. *Journal of Research of the National Bureau of Standards.* 27:191-6.

[20] Beck MW. A Preliminary Investigation into the Si/$BaSO_4$ Combustion Mechanism. ICI Explosives Group Technical Report No 684. Ardeer Site1989.

[21] Miklaszewski EJ, Poret JC, Shaw AP, Son SF, Groven LJ. 2014 Ti/C-3Ni/Al as a Replacement Time Delay Composition. *Propellants, Explosives, Pyrotechnics*. 39:138-47.

[22] Ellern H. Military and Civilian Pyrotechnics. New York: Chemical Publishing Company; 1968.

[23] Charsley EL, Chen C-H, Boddington T, Laye PG, Pude JRG. 1980 Differential thermal analysis and temperature profile analysis of pyrotechnic delay systems: ternary mixtures of silicon, boron and potassium dichromate. *Thermochimica Acta*. 35:141-52.

[24] UN Recommendations on the Transport of Dangerous Goods. Model Regulations. In: Nations U, editor. 15 ed. New York and Geneva: United Nations; 2007.

[25] Kosanke KLK, B. J.; Sturman, B. T.; Winokur, R. M. Encyclopedic Dictionary of Pyrotechnics: (and Related Subjects): *Journal of Pyrotechnics*, Incorporated; 2012.

[26] Rai M, Mountjoy G. 2014 Molecular dynamics modelling of the structure of barium silicate glasses BaO-SiO_2. *Journal of Non-Crystalline Solids*. 401:159-63.

[27] Tyurnina ZG, Lopatin SI, Shugurov SM, Stolyarova VL. 2006 Thermodynamic properties of silicate glasses and melts: I. System BaO-SiO_2. *Russian Journal of General Chemistry*. 76:1522-30.

[28] Hopwood JD, Mann S. 1997 Synthesis of Barium Sulfate Nanoparticles and Nanofilaments in Reverse Micelles and Microemulsions. *Chemistry of Materials*. 9:1819-28.

[29] Hesse K-FL, F. 1980 Crystal chemistry of silica-rich barium silicates. *Zeitschrift für Kristallographie*. 153:3-17.

[30] Grebenshchikov RGT, N. A. 1962 New data on the barium oxide-silica phase diagram. *Bulletin of the Academy of Sciences of the USSR Division of Chemical Science*. 11:503-9

[31] Boulay E, Nakano J, Turner S, Idrissi H, Schryvers D, Godet S. 2014 Critical assessments and thermodynamic modeling of BaO–SiO_2 and SiO_2–TiO_2 systems and their extensions into liquid immiscibility in the BaO–SiO_2–TiO_2 system. *Calphad*.47:68-82.

[32] Tashiro C, Yamada H, Akiba T, Nawata S. 1976 Study on the hydration of 2BaO·SiO_2. *Cement and Concrete Research*. 6:633-40.

[33] WHO. World Health Organization (Water Sanitation and Health) Barium in drinking-water; Background document for development of WHO Guidelines for Drinking-water Quality , WHO/SDE/WSH/03.04/76 2004.

[34] Jacobs IA, Taddeo J, Kelly K, Valenziano C. 2002 Poisoning as a result of barium styphnate explosion. *American Journal of Industrial Medicine*. 41:285-8.